Microsyst Technol (2014) 20:793–802
DOI 10.1007/s00542-013-2035-1

TECHNICAL PAPER

Magnetic tunnel junction sensors with pTesla sensitivity

S. Cardoso · D. C. Leitao · L. Gameiro · F. Cardoso · R. Ferreira · E. Paz · P. P. Freitas

Received: 2 August 2013 / Accepted: 7 December 2013 / Published online: 21 January 2014

Abstract Ultrasensitive magnetic field sensors at low frequencies are necessary for several biomedical applications. Suitable devices can be achieved by using large area magnetic tunnel junction (MTJ) sensors combined with permanent magnets to stabilize the magnetic configuration of the free layer and improve linearity. However, further increase in sensitivity and consequently detectivity are achieved by incorporating also soft ferromagnetic flux guides (FG). A detailed study of tunnel junction sensors with variable areas and aspect ratios is presented in this work. In addition, the effect in the sensors transfer curve, namely in their coercivity and sensitivity, as a consequence of the incorporation of permanent magnets and FG is also thoroughly discussed. Devices consisting of MgO-based MTJ with magnetoresistance levels of ~200 %, and incorporating thin film permanent magnets (CoCrPt) and CoZrNb flux guides, could reach sensitivities of ~2,000 %/mT at room temperature, in a non-shielded environment. The noise levels of the final device measured at 10 Hz yield 3.9×10^{-17} V^2/Hz, leading to the lowest detectable field of ~49 pT/Hz$^{0.5}$. This value is half of the best value we obtained with MTJ-based devices, and represents a step further towards integration in a biomedical device for magnetocardiography.

S. Cardoso (✉) · D. C. Leitao · L. Gameiro · F. Cardoso · P. P. Freitas
INESC-MN and IN, Rua Alves Redol 9, 1000-029 Lisbon, Portugal
e-mail: scardoso@inesc-mn.pt

S. Cardoso
Departamento de Física, Instituto Superior Técnico (IST), Universidade de Lisboa - UL, Av. Rovisco Pais, 1000-029 Lisbon, Portugal

R. Ferreira · E. Paz · P. P. Freitas
INL International Iberian Nanotechnology Laboratory, Av. Mestre José Veiga, 4715-31 Braga, Portugal

1 Introduction

Biomedical imaging techniques such as magneto-cardiography demand highly sensitive magnetic sensors capable to detect fields down to sub-picoTesla range at low frequencies (<10 Hz). Currently, systems composed of superconducting quantum interference devices or hybrid supercond ucting/magnetoresistive (MR) sensors fulfill such requirements, with the inconvenient of working at temperatures a few degrees above absolute zero, having the necessity of a cryogenic apparatus (Pannetier-Lecoeur et al. 2011). As an alternative, magnetic field detection at room temperature has been validated for ultra-low fields using MR sensors, which have proven to be a reliable tool in hard disk magnetic recording. From the several MR sensor technologies available presently, magnetic tunnel junctions (MTJ) based on MgO barriers (Ikeda et al. 2008) are highlighted as the most competitive sensors aiming pT detection at room temperature. Table 1 summarizes key characteristics obtained with several sensing architectures, aiming ultra-low magnetic field detection. Our group demonstrated detection limits in the pT/$\sqrt{\text{Hz}}$ range by coupling MR and MTJ sensors to magnetic flux guides (FG) (Chaves et al. 2007; Leitao et al. 2012) without a significant increase in the noise levels (Almeida and Freitas 2009). Typical high permeability materials for FGs such as NiFe or (amorphous) Co-based alloys are currently used in distinct applications, namely in recessed MR heads (Tsang et al. 1992), highly sensitive spin-valves, MTJs and Hall sensor devices (Chaves et al. 2007; Guedes et al. 2007; Prieto et al. 2002; Freitas et al. 1999), and also in magnetic multilayers and

Table 1 Summary of characteristics and achievements of competing technologies (based on magnetoresistance) for ultra-low field detection

Active sensor	Details	Magnetic flux guides	Operation temperature	Detectivity at 1 Hz (T/Hz$^{0.5}$)	Device footprint	Reference
AMR-bridge	Honeywell comercial AMR HMC1001	N	RT	100 pT	N/A	Stutzke et al. (2005)
GMR-bridge	NVE commercial GMR devices	Y	RT	4 nT	N/A	Stutzke et al. (2005)
GMR-single	Spin valves with ferromagnetic FGs	Y	RT	7–20 nT	>470 × 400 μm^{2b}	Leitao et al. (2012); Guedes et al. (2007)
GMR-single	Spin valves with MEMs–FGs	Y	RT	40–600 nT[a]	900 × 2,400 μm^{2b}	Guedes et al. (2008, 2012)
GMR-single	*Spin-valve with YBaCuO loop*	*Y*	*77 K*	*~200 fT*	*3 × 3 cm^{2c}*	*Pannetier et al.* (2004)
GMR-bridge	*GMR wheatstone bridge with Nb loop*	*Y*	*4 K*	*3 pT*	*3 × 3 cm^{2c}*	*Pannetier-Lecoeur et al.* (2011)
TMR-single	MTJ	N	RT	350 nT	N/A	Mazumdar et al. (2007)
TMR-bridge	NVE SDT	N	RT	~4 nT	N/A	Stutzke et al. (2005)
TMR-series	MTJ series	N	RT	16.2 nT	500 × 500 μm^2	Guerrero et al. (2009)
TMR-single	Al_2O_3 MTJ with ferromagnetic FGs	Y	RT	534 pT	2,210 × 1,775 μm^{2b}	Jander et al. (2003)
TMR-single	MgO MTJ sensor with ferromagnetic FGs	Y	RT	300 pT	500 × 500 μm^{2b}	Chaves et al. (2007, 2011)

Highlighted (italics) are the devices operating at low temperature

[a] Requires scheme to modulated low frequency fields

[b] Defined by FGs size

[c] Defined by superconducting loop size

colossal MR materials with increased low-field magnetoresistance (Yuan et al. 2002).

For ultra-low field applications, not only large output voltages are required (for larger output signals) but also large signal-to-noise ratio (SNR). The main sources of noise in MTJs arise from 1/f noise, thermal noise and shot noise (Ingvarson et al. 2000), as follows:

$$S_v\left(\frac{V^2}{Hz}\right) = S_{1/f} + S_{WBN} = \frac{\alpha_H I_{bias}^2 R^2}{Af} + 2eI_{bias}R^2 \coth\left(\frac{eV_{bias}}{2k_BT}\right),$$

where S_v stands for the noise spectral density, α_H for the modified Hooge constant for MTJs, I_{bias} (V_{bias}) the bias current (voltage), R the resistance, A the area of the sensor, f the frequency, e the electron charge, k_B the Boltzmann constant and T the temperature. In the low frequency range (<1 kHz), the *1/f* noise becomes dominant, which limits the performance of the device (Edelstein and Fischer 2002). For medical imaging applications where the low frequency field sources cannot be modulated, one has to follow a different route to suppress this low frequency noise. Proposed mechanisms resort to superconducting loops (Pannetier et al. 2004) or microelectromechanical cantilever-system incorporating a FG structure (Edelstein and Fischer 2002; Guedes et al. 2008, 2012).

Previous work in our group proposed to use MTJ sensors with integrated magnetic FGs which increase the sensitivity of the sensor by amplifying locally the magnetic fields that reaches the sensing layer (Chaves et al. 2007; Leitao et al. 2012; Guedes et al. 2007). In this paper we present devices based on high resistance MTJ, showing magnetoresistance levels (TMR) of ~200 %. Several groups working on state-of-the-art MTJ materials have addressed the difficulty in obtaining sensor transfer curves (TMR versus external field) showing simultaneously high TMR levels (>200 %), low coercivity (<0.2 mT) and high sensitivity (S > 10 %/Oe). We have previously optimized structures based on ultrathin CoFeB free layers (Wisniowski et al. 2008), or incorporating a self aligned permanent magnet bias (Chaves et al. 2011), or improved magnetic flux concentrators (Marinho et al. 2011). In this paper, we selected a material stack based on CoFeB/NiFe free layers, which was optimized for reduced coercivity while maintaining the full TMR of 200 % measured in single CoFeB free layer stacks. The sensor geometry has been optimized so that lateral permanent magnets

and magnetic FG are incorporated, therefore enhancing the sensor sensitivity, which has a major impact on the noise characteristics. The noise spectra provide information on the sensor detection limits (detectivity) and expectations for an application in biomedical imaging. This application is particularly challenging because requires low detectivities at a frequency range (DC-100 Hz) where the MR sensors have their largest noise levels. Finally, the selection of sensor architecture needs to be driven by the spatial resolution required for each application. From Table 1 one can see that optimized detectivities with TMR sensors are associated to large footprint devices.

2 Experimental details

Figure 1 summarizes the device architecture used for this work, which has been described previously (Cardoso et al. 2013). The MgO-based MTJ stack was deposited at INL by sputtering in a Singulus Timaris tool, with the following structure: Si/SiO_2/Ta 5/CuN 50/Ta 3/CuN 50/Ta 3/Ru 5/$Ir_{20}Mn_{80}$ 7.5/$Co_{70}Fe_{30}$ 2/Ru 0.85/$Co_{40}Fe_{40}B_{20}$ 2.6/MgO 1/$Co_{40}Fe_{40}B_{20}$ 3/Ta 0.21/$Ni_{80}Fe_{20}$ 16/Ta 10/CuN 30/Ru 7 (thickness in nm) (Chaves et al. 2011). The full MTJ stack was patterned at INESC-MN by optical lithography and ion milling etching, to define the bottom electrode and the sensor elements, which consist on rectangular, square and circular pillars with areas ranging from ~30 up to 1,500 μm^2. A 100 nm thick Al_2O_3 layer was deposited by RF sputtering for passivation and lateral insulation of the MTJ pillar.

Magnetic FGs were incorporated into the device, consisting of 600 nm thick sputtered amorphous $Co_{93}Zr_{16}Nb_3$ (CZN) film patterned by optical lithography and lift-off. Separation between poles and sensor was set to 2 μm. Therefore the effective gap between FG poles will vary with the sensor height (h), ranging from 6 to 42 μm. During the deposition process an uniaxial anisotropy axis parallel to the gap was induced in the FGs by applying an in-plane magnetic field.

Free layer stabilization was partially achieved by integrating $Co_{66}Cr_{16}Pt_{18}$ permanent magnet thin film element (PM) (Chaves et al. 2011) defined by optical lithography and lift-off with a thickness of 120 nm, and with a separation to sensor of 2 μm on each side (therefore, adjustable gap, for each MTJ geometry). A 300 nm thick SiO_2 passivation layer was then deposited, and vias to the MTJ pillar were opened by reactive ion etching, prior to the final metallization step, using 300 nm thick AlSiCu contacts protected

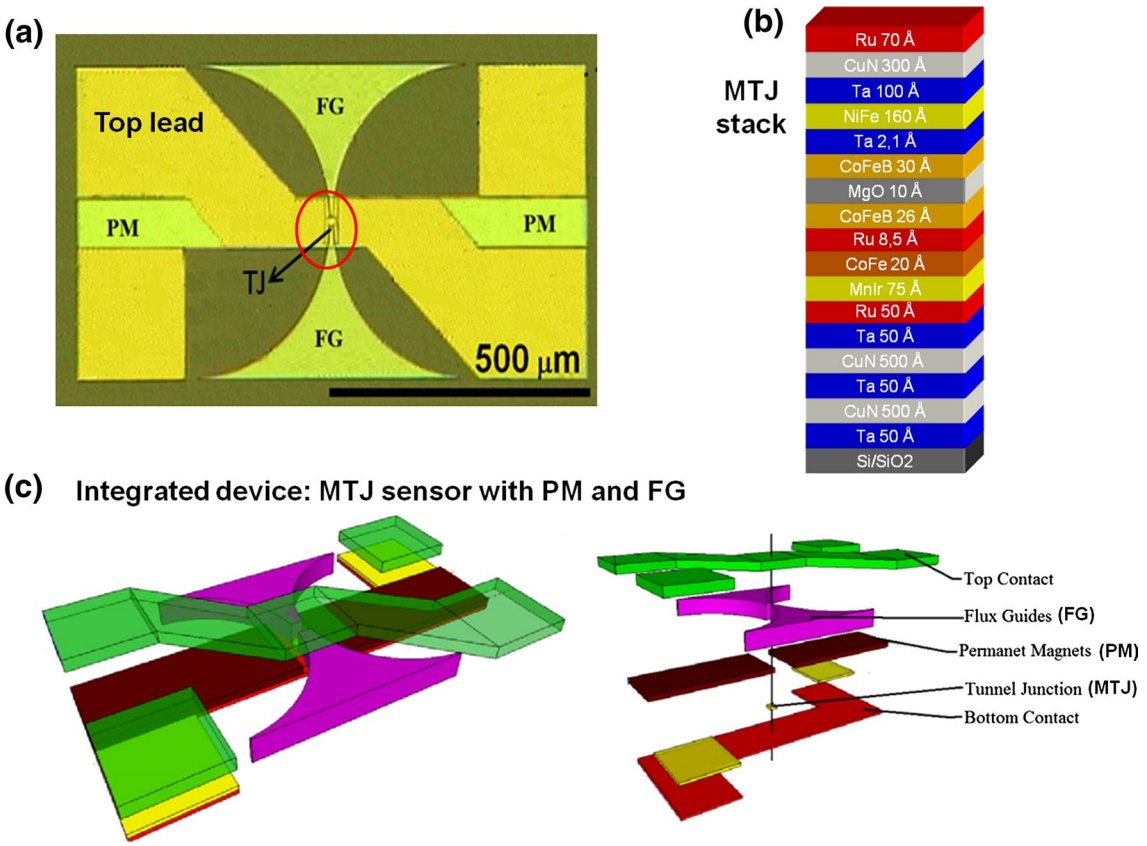

Fig. 1 **a** Top-view picture of one device measured in this paper, based on the MTJ stacks described in (**b**). **c** Layout of the final MTJ sensor, consisting of a four contact device with free layer stabilization using permanent magnets (PM) and incorporation of flux guides (FG)

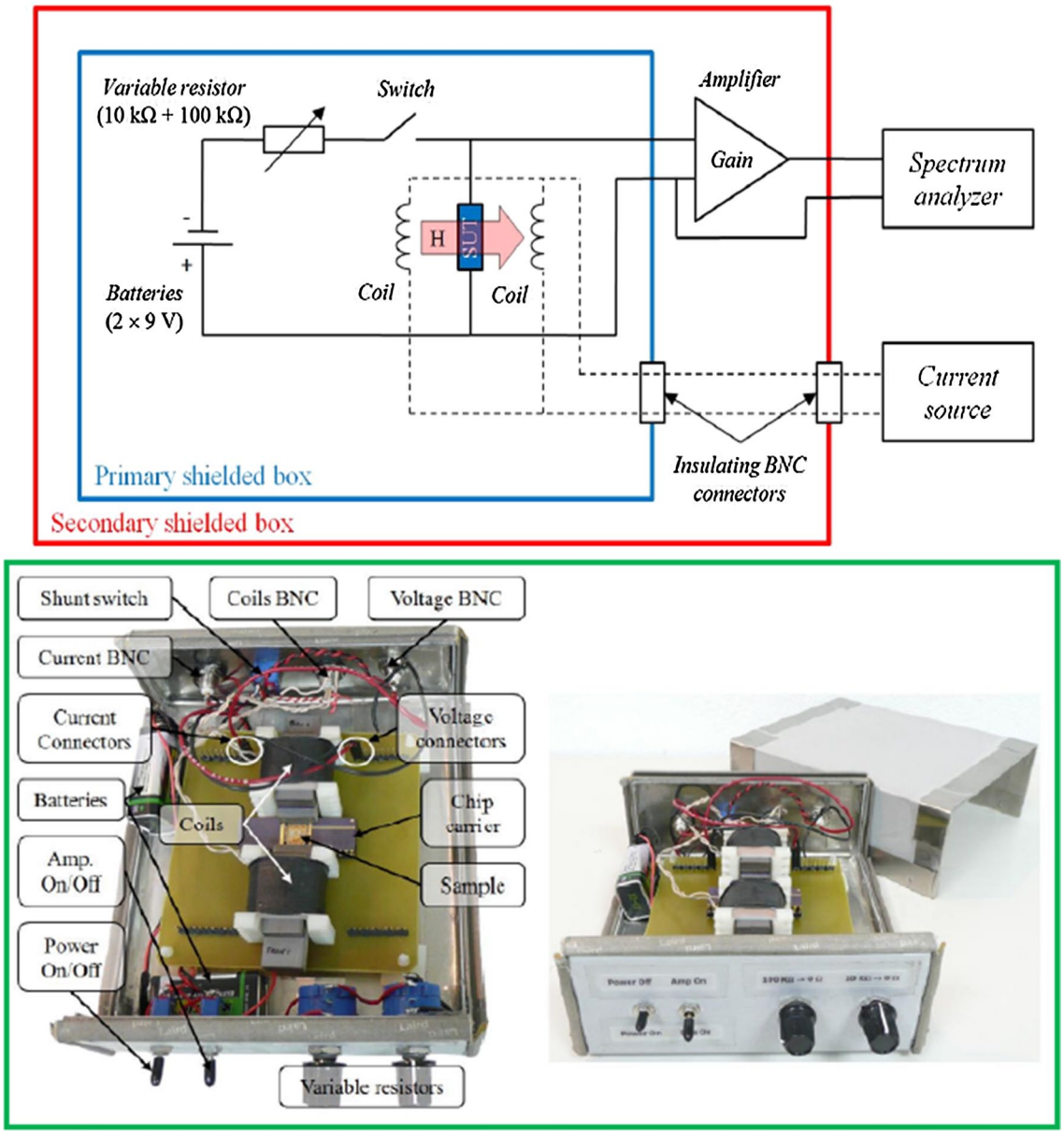

Fig. 2 *Top* layout of the noise measurement system (Ferreira et al. 2006) where the sample is placed between the coils (labelled as SUT-sample under test). *Bottom* picture of the shielded box where the encapsulated sensors are mounted, and characterized

with a 15 nm thick TiWN cap layer. The deposited stack was annealed at 360 °C in vacuum for 1 h and cooled down under a 1 T in-plane DC magnetic field. Prior to microfabrication, current-in-plane-tunneling (CIPT–CAPRES system at INL) measurements on unpatterned stacks revealed an average TMR = 200 % and maximum resistance-area product of $R \times A = 7{,}600\ \Omega\ \mu m^2$. Device transfer curves were measured by a dc four probe method and magnetic characterizations [M(H)] were performed by a vibrating sample magnetometer (VSM), both at room temperature. The noise characterization was performed after wire bonding the devices into a chip carrier, using a battery supplied current source, in a μ-metal-shielded box. Figure 2 displays the setup used for the noise characterization, which is described in Ref (Ferreira et al. 2006). The noise power spectrum was amplified by a FEMTO DLPVA-100-BLN-S in a range of DC-100 kHz and measured by a Tektronix RSA3308A real-time spectrum analyzer.

3 Experimental results

Figure 3a summarizes the values of TMR obtained for the sensors characterized here (more than 200 devices), where

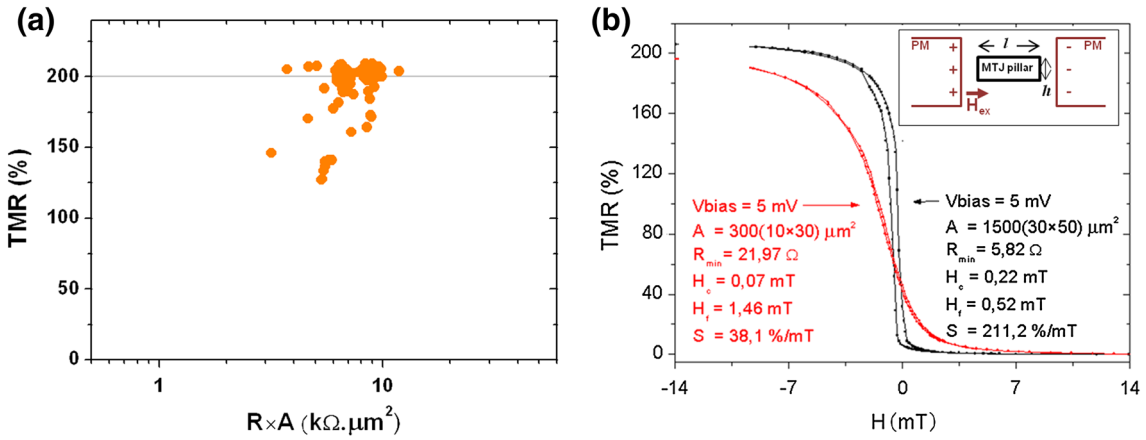

Fig. 3 **a** Statistics over the several devices measured (more than 200), with different geometries (*squares, circles, rectangles*), including devices with PM and FG or without PM or FG. **b** Example of a complete device transfer curve, corresponding to sensors with *rectangular shape* ($l = 50$ μm, $h = 30$ μm and $l = 10$ μm, $h = 30$ μm), incorporating PM elements (color figure online)

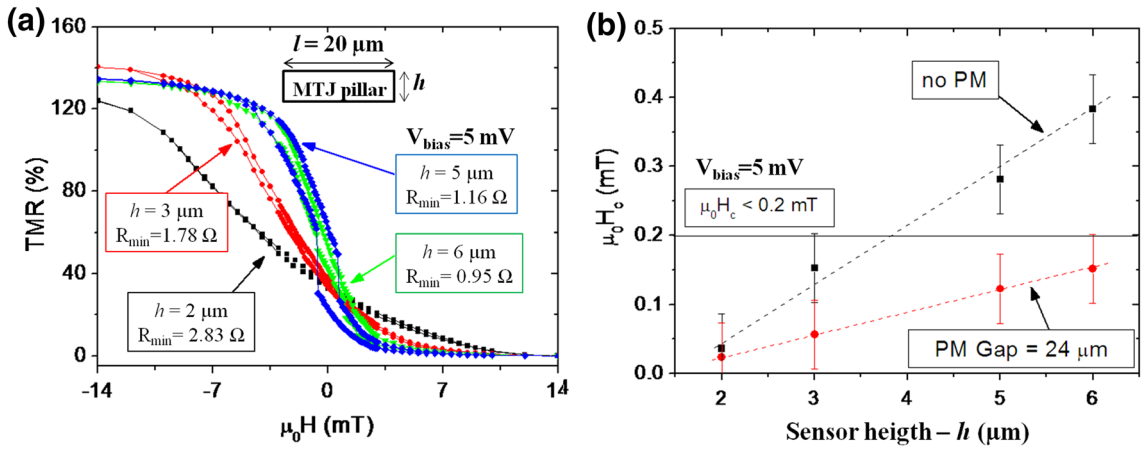

Fig. 4 **a** Transfer curves of MTJ sensors (no PM, no FG) with high aspect ratio: *rectangular shape*, fixed length ($l = 20$ μm) and variable width ($h = 2$–6 μm). **b** $\mu_0 H_c$ dependence on the sensor height. Here the effect of the PM biasing is clear in reducing the coercivity, therefore allowing the use of larger sensors with a perfect linear curve, rather than being limited to narrow dimensions ($h \leq 3$ μm). Each data point displays the average $\mu_0 H_c$ values obtained from measurements of several devices, with corresponding mean deviation (*error bars*)

the 200 % value measured at the unpatterned stack could be obtained also for the final devices, denoting a successful microfabrication process. Figure 3b shows one example of two devices transfer curves with a linear signature, and where the effect of the dimensions (h) on the sensitivity is clearly observed. Also, an average shift in the transfer curve center of ~−0.66 mT was observed in all sensors measured, and includes effects from the pinned layer demagnetizing field, but arises mainly from ferromagnetic Néel coupling.

In fact, the performance of the MTJ sensors is strongly dependent on the linear characteristics of their transfer curves. For improved field detectivities, obtaining a highly sensitive transfer curve (large slope) and coherent free layer magnetization rotation (no Barkhausen-noise) are key factors. In this work, the choice of the free layer composition was linked to the geometry of the MTJ. The linearization for high aspect ratio rectangular shape MTJ sensors was achieved by setting the pinned layer (PL) and free-layer (FL) magnetization orthogonal to each other guaranteeing that $l \gg$ h, causing a strong shape anisotropy and forcing the FL magnetization to lie along the length (l) of the sensor. The demagnetizing field of the FL layer is given by $H_d^{FL} = \mu_0 M_s^{FL} t^{FL} / h$ (Leitao et al. 2012), where M_s is the FL the saturation magnetization and t the FL thickness.

While analyzing the experimental data we consider a sensor to be linear when $\mu_0 H_c$ is lower than 0.2 mT (dashed line in Fig. 4b). We have observed (as expected) that narrower sensors ($h = 2$ μm) showed a linear response with

low coercivity, $\mu_0 H_c = 0.03$ mT (Fig. 4a). For the sensors with the larger heights, a higher coercivity was obtained instead ($\mu_0 H_c = 0.4$ mT) consistent with the presence of magnetization rotation processes and domain wall motion consequence of a smaller FL demagnetizing field [$\mu_0 H_d \approx 4$ mT for $h = 5$ μm; $M_s(Ni_{80}Fe_{20}) = 800$ kA/m; $M_s(Co_{40}Fe_{40}B_{20}) = 1{,}100$ kA/m;] which leads to deviations from the expected orthogonal magnetization configurations between FL and PL (Fig. 4a). Such behavior can also lead to discontinuities in the transfer curve usually associated with domain wall pinning and de-pinning at low anisotropy sites (e.g. defects, borders), as observed in the $h = 5$ μm curve.

The sensitivity (S) of the sensor is defined in the linear operation range of the transfer curve as $S = TMR/2\mu_0 H_{sat}$, with H_{sat} being the saturation field usually given by $H_{sat} = H_k + H_d$, and where H_k is the intrinsic anisotropy field (~few mT). For example, if h = 5 μm, then $\mu_0 H_{sat} \approx 3.25$ mT is extracted from the transfer curves (Fig. 4a). This value is smaller but consistent with the calculated H_d due to the deviation from purely linear behavior without hysteresis. The sensor sensitivity can be rewritten as (Trindade et al. 2008):

$$S = \frac{TMR}{2[\mu_0 H_k + \mu_0 H_d]} \propto TMR \times h \left[\%/\mathrm{mT}\right].$$

Therefore, when $l \gg h$ (high aspect ratio) the sensitivity shows a linear dependence on the sensor h (Cardoso et al. 2013). However, deviations from this trend are clear when $l \sim> h$, which is the case for the majority of the sensors described in this paper.

3.1 Biasing with permanent magnets

For geometries with low aspect-ratio (i.e. squares, circles), the MTJ sensors require an appropriated longitudinal bias field (LB) set in the free layer to assure a hysteresis-free, linear, symmetric transfer curves with suppressed magnetic noise. Such a LB field suppresses multidomain formation in the sensing layer which induces Barkhausen noise in the sensor transfer curve (Chaves et al. 2011; Yamada et al. 1990). Distinct approaches can be used, such as incorporated permanent magnets (PM) or exchange coupled free layers (Ferreira et al. 2012; Chen et al. 2012). In this work, FL stabilization is partially achieved by integrating the CoCrPt PM. Unpatterned M(H) loops exhibited a $\mu_0 H_c = 61.7$ mT, M_s ~ 997 kA/m and remanence of $M_r t = 0.9$ memu/cm^2.

High LB fields result in improved sensing layer stability, leading however to lower field sensitivities of the sensor (Ho et al. 2004). Therefore the PM elements were optimized, and pattern into rectangular shapes with a length of 450 μm, width of 80 μm, and are expected to create a bias field ($\mu_0 H_{LB}$) at the center of their gap of ~3.5 mT (example for a 24 μm gap PM).

Despite the reduction in sensor sensitivity, the need for PM is fully justified since an overall reduction in device coercivity is visible when PMs are used, indicating that a LB favors a coherent rotation of the FL. Figure 5 shows clearly the impact of using a PM linearization scheme. Upon analyzing the transfer curves for all devices microfabricated with PM biasing elements, we could see that $\mu_0 H_c$ <0.2 mT irrespectively of MTJ sensor's dimensions and shape (square, rectangle or circle).

3.2 Enhanced sensitivity with magnetic flux guides

Magnetic FGs are used to increase the sensitivity of the MTJ by amplifying in gap the field that reaches the sensitive part of the sensor. M(H) curves of unpatterned CZN film used here as FG material, displayed in the hard-axis

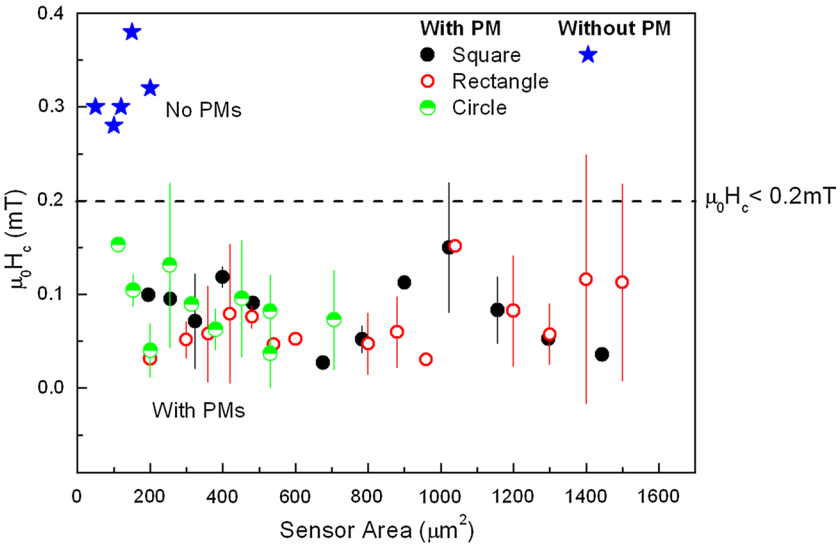

Fig. 5 Statistics on the transfer curve coercivity values ($\mu_0 H_c$) measured for sensors patterned with several geometries (*square, rectangle* and *circles*) and dimensions. The incorporation of permanent magnets (in contrast with some examples in *blue*) is clearly an efficient method to improve linearity, even for larger sensor areas. The devices showed have no FGs. Each data point displays the average $\mu_0 H_c$ values obtained from measurements of several devices, with corresponding mean deviation (*error bars*)

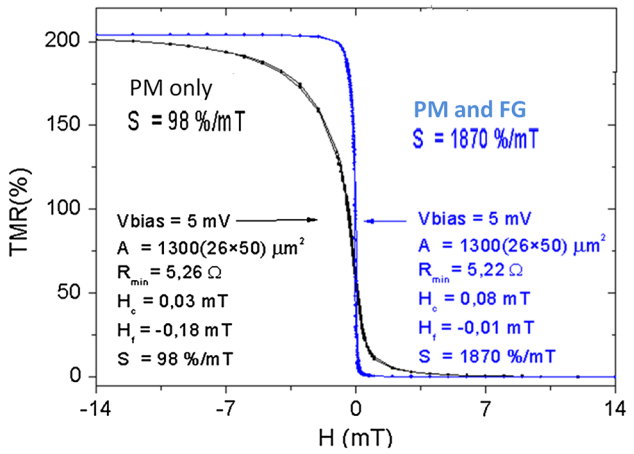

Fig. 6 Transfer curves of MTJ sensor with and without FGs ($h = l = 16$ μm); both sensors have incorporated PMs

a linear behavior with anisotropy field $\mu_0 H_k \approx 2.16$ mT, $M_s \approx 913$ kA/m and $\chi = 685$. Additionally, a $\mu_0 H_c \approx 0.025$ mT and $\mu_0 H_{sat} \approx 0.32$ mT were obtained for the easy-axis configurations. The patterned FGs show an entrance width of 500 μm, and a total length of 250 μm. This geometry is compatible with a compact, intermediate footprint device. The distance between the sensor and FG pole was fixed in 2 μm, leading to gaps (pole–pole distance) ranging from 6 to 42 μm depending on the sensor height (h). Notice that, the field amplification effect in gap is first a geometric effect, increasing linearly with the length of the FG, and decreasing for larger gaps.

Figure 6 compares the transfer curve of MTJ sensors with and without FGs. The inclusion of FGs leads to a more steep transfer curve, corresponding to an increase in sensitivity of ~19 times. The gain in sensitivity is defined as the ratio between the sensitivity of the sensor with FGs and PMs to the same sensor sensitivity without FGs nor PMs [$S_{FG,\,PM}/S_{no\ FG,\,no\ PM}$].

Another striking feature when FGs are included is a clear enhancement in H_c. The origin of this hysteresis is not completely clear, arising most probably from magnetostatic coupling between FG poles and the sensor (Leitao et al. 2012; Trindade et al. 2009), thus hindering FL reversal.

Figure 7a compares the impact of the MTJ geometry on device sensitivity, and its dependence on the sensor area (for devices with PM, but without FG). The effectiveness of FG is highlighted in Fig. 7b, where it can be seen on the increase in the sensors' sensitivity by 15 × upon incorporation of FG in the sensor layout. Nevertheless, a gain in the sensitivity provided by the incorporated FGs ranging from 14 up to 26 times was achieved for the sensors discussed here, with maximum sensitivity levels of ~2,000 %/mT.

3.3 Noise level characterization

Figure 8a shows the noise spectra measurements for a selected MTJ with large area (low aspect ratio). This structure corresponds to $l = 50$ μm and $h = 30$ μm, including both PMs and FGs and displaying a TMR = 206 %, $R_{min} = 5.6$ Ω and S = 1,860 %/mT at bias voltage of $V_{bias} = 5$ mV. A sensor noise level for the final device of $S_v = 3.9 \times 10^{-17}$ V²/Hz at 10 Hz was achieved. Also, for the sensor with FGs the 1/f noise corner was observed

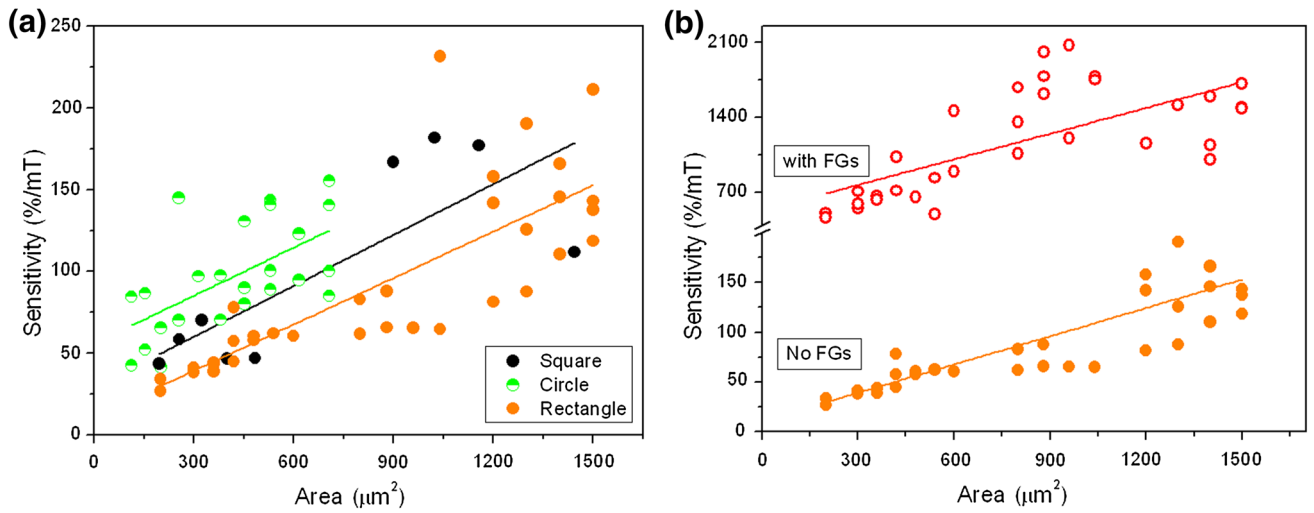

Fig. 7 **a** Sensitivity dependence on MTJ sensor area, obtained from the transfer curves measured for *rectangular, circular and squared* devices. **b** Enhanced sensitivity is clearly achieved upon incorporation of magnetic FG, here demonstrated for rectangular sensors. We recall that the separation between FG poles and sensor was set to 2 μm and consequently the effective gap between FG poles will vary with the sensor h (Fig. 9)

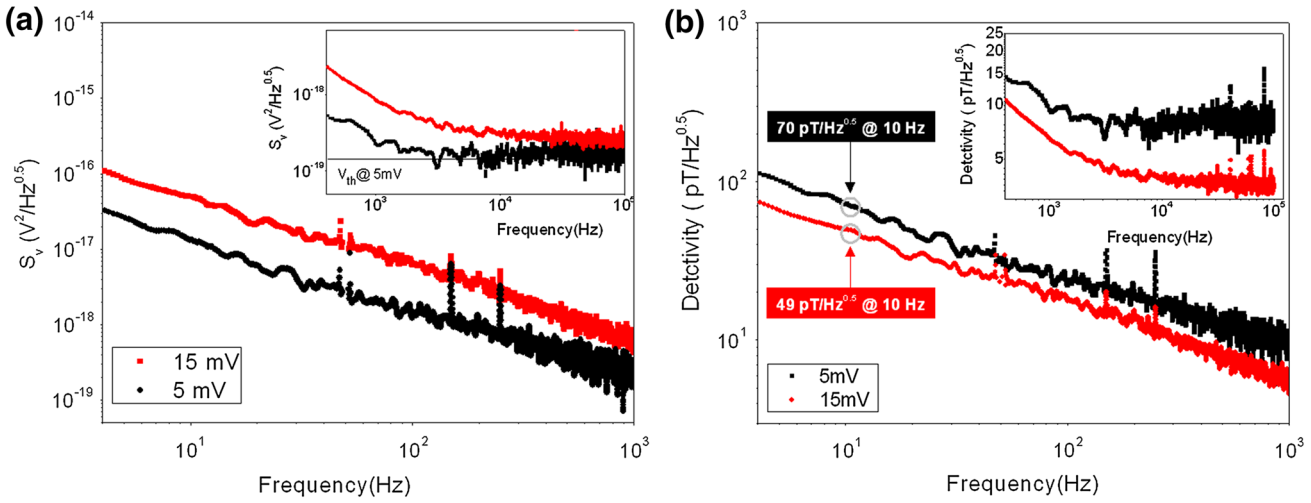

Fig. 8 **a** Noise spectra and **b** detectivity for a selected MTJ sensor with PMs and FGs ($l = 50$ μm, $h = 30$ μm). Measurements were done with 5 and 15 mV bias voltages at the junction terminals

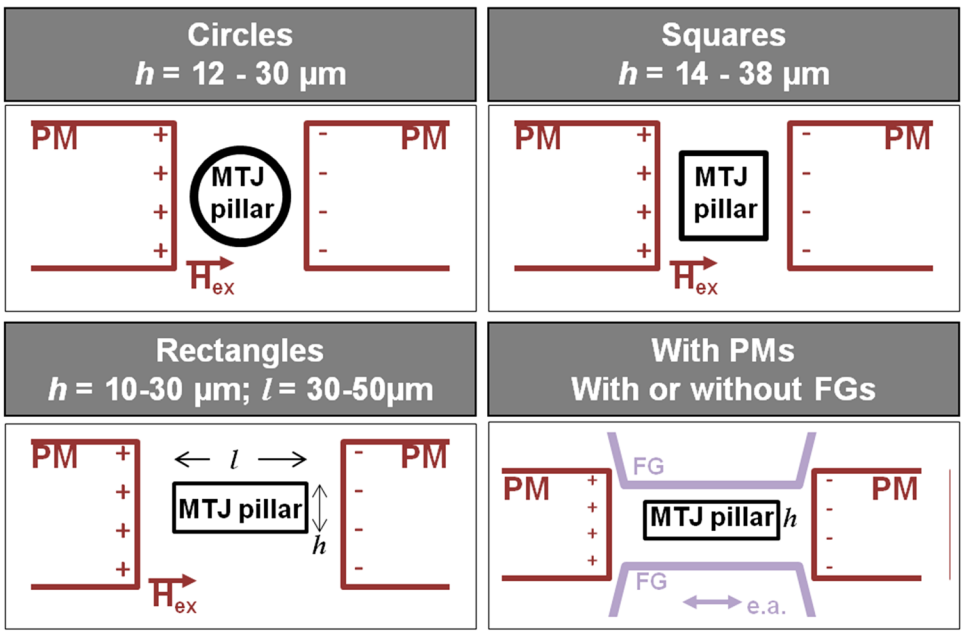

Fig. 9 Geometries used for the sensing element (MTJ pillar) patterned into rectangles ($h \times l$ = height × length), *circles* and *squares*, using similar PM elements. Separation between PM poles was adjusted for each geometry, to set a fixed 2 μm separation between PM and the MTJ element

at ~1.2 kHz for $V_{bias} = 5$ mV. The Hooge parameter (α_H) in the linear region was similar in both cases (with and without FGs) giving α_H of about 3×10^{-8} μm^2, indicating that no additional contribution of the magnetic noise appears with the inclusion of FG (Chaves et al. 2007; Leitao et al. 2012; Almeida and Freitas 2009). However, this α_H value is one order of magnitude higher than previously reported for similar devices (Chaves et al. 2007), reflecting a higher intrinsic noise of the MTJ stack.

Figure 8b shows the detectivity spectra of the noise measurements. In the low frequency range these sensors shows a detectivity of ~1,800 pT/Hz$^{0.5}$ at 10 Hz without FG as previously reported (Cardoso et al.2013). With the inclusion of FGs a significant improvement in detectivity is observed with 49 pT/Hz$^{0.5}$ at 10 Hz. This result reflects an increase in detection capability in ~2 times compared to our previous published papers. Such enhancement was obtained by optimization of the MTJ materials, together with the use of sensors with very large areas and low aspect ratios.

An estimation of the detection level at 1 Hz (envisaged operation point) is obtained from linear extrapolation, giving ~155 pT/Hz$^{0.5}$ for the final device with PMs and FGs. At high frequencies (>100 kHz) smaller detectivity values are obtained, namely ~3.5 pT/Hz$^{0.5}$.

4 Conclusions

This work summarizes the optimization steps of integrated devices towards pT field detection capability at room temperature. Such devices rely on three key elements: (1) state-of-the-art MgO-MTJ sensors with TMR reaching 200 % and low coercivity, (2) permanent magnets as a mean to promote free-layer stabilization, despite the drawback of reducing the field sensitivity of the sensor and (3) magnetic FG for improved sensitivity. In particular the magnetic free-layer was optimized (CoFeB/NiFe combination, rather than a single CoFeB) to decrease the intrinsic noise levels of the sensor. A detailed study on the influence of the junction dimensions and aspect ratio in the transfer curve coercivity and sensitivity is presented targeting at the best feature for improved final detectivity of the device. For larger areas and low aspect ratio devices, sensitivity levels in excess of 2,000 %/mT were demonstrated allowing one to reach detectivities of ~46 $pT/Hz^{0.5}$.

Acknowledgments D. C. Leitao is thankful to FCT for the grant SFRH/BPD/72359/2010. F. Cardoso acknowledges funding from IMAGIC EU-FP7-ICT-288381. INL acknowledges partial funding from the ON2 project from PO Norte. INESC-MN acknowledges FCT funding through the Instituto de Nanociência e Nanotecnologia (IN) Associated Laboratory.

References

Almeida JM, Freitas PP (2009) Field detection in MgO magnetic tunnel junctions with superparamagnetic free layer and magnetic flux concentrators. J Appl Phys 105:07E722. doi:10.1063/1.3077228

Cardoso S, Gameiro L, Leitao DC, Cardoso F, Ferreira R, Paz E, Freitas PP (2013) Magnetic tunnel junction sensors with pTesla sensitivity for biomedical imaging. Proc. SPIE microtechnologies 8763, smart sensors, actuators, and MEMS VI, 87631[a]. doi:10.1117/12.2018070

Chaves RC, Freitas PP, Ocker B, Maass W (2007) Low frequency picotesla field detection using hybrid MgO based tunnel sensors. Appl Phys Lett 91:102504. doi:10.1063/1.2775802

Chaves RC, Cardoso S, Ferreira R, Freitas PP (2011) Low aspect ratio micron size tunnel magnetoresistance sensors with permanent magnet biasing integrated in the top lead. J Appl Phys 109:07E506. doi:10.1063/1.3537926

Chen JY, Feng JF, Coey JMD (2012) Tunable linear magnetoresistance in MgO magnetic tunnel junction sensors using two pinned CoFeB electrodes. Appl Phys Lett 100:142407. doi:10.1063/1.3701277

Edelstein AS, Fischer GA (2002) Minimizing 1/f noise in magnetic sensors using a microelectromechanical system flux concentrator. J Appl Phys 91:7795. doi:10.1063/1.1451901

Ferreira R, Wisniowski P, Freitas PP, Langer J, Ocker B, Maass W (2006) Tuning of MgO barrier magnetic tunnel junction bias current for picotesla magnetic field detection. J Appl Phys 99:08K706. doi:10.1063/1.2173636

Ferreira R, Paz E, Freitas PP, Wang J, Xue S (2012) Large area and low aspect ratio linear magnetic tunnel junctions with a soft-pinned sensing layer. IEEE Trans Mag 48:3719. doi:10.1109/TMAG.2012.2200468

Freitas PP, Costa JL, Almeida N, Melo LV, Silva F, Bernardo J, Santos C (1999) Giant magnetoresistive sensors for rotational speed control. J Appl Phys 85:5459. doi:10.1063/1.369975

Guedes A, Almeida JM, Cardoso S, Ferreira R, Freitas PP (2007) Improving magnetic field detection limits of spin valve sensors using magnetic flux guide concentrators. IEEE Trans Magn 43:2376–2378. doi:10.1109/TMAG.2007.893119

Guedes A, Patil SB, Cardoso S, Chu V, Conde JP, Freitas PP (2008) Hybrid magnetoresistive/microelectromechanical devices for static field modulation and sensor 1/f noise cancellation. J Appl Phys 103:07E924–07E933. doi:10.1063/1.2837661

Guedes A, Jaramillo G, Buffa C, Vigevani G, Cardoso S, Leitao DC, Freitas PP (2012) Towards picoTesla magnetic field detection using a GMR-MEMS hybrid device. IEEE Trans Magn 48:4115–4118. doi:10.1109/TMAG.2012.2203297

Guerrero R, Pannetier-Lecoeur M, Fermon C, Cardoso S, Ferreira R, Freitas PP (2009) Low frequency noise in arrays of magnetic tunnel junctions connected in series and parallel. J Appl Phys 105:113922. doi:10.1063/1.3139284

Ho MK, Ching T, Childress J, Fontana R, Katine J, Carey K (2004) Study of longitudinal stabilization using in-stack biasing. IEEE Trans Magn 40:189. doi:10.1109/TMAG.2003.821201

Ikeda S, Hayakawa J, Ashizawa Y, Lee YM, Miura K, Hasegawa H, Tsunoda M, Matsukura F, Ohno H (2008) Tunnel magnetoresistance of 604 % at by suppression of Ta diffusion in pseudo-spin-valves annealed at high temperature. Appl Phys Lett 93:082508. doi:10.1063/1.2976435

Ingvarson S, Xiao G, Parkin S, Gallagher W, Grinstein G, Koch R (2000) Low-frequency magnetic noise in micron-scale magnetic tunnel junctions. Phys Rev Lett 85:3289. doi:10.1103/PhysRevLett.85.3289

Jander A, Nordman CA, Pohm AV, Anderson JM (2003) Chopping techniques for low-frequency nanotesla spin-dependent tunneling field sensors. J Appl Phys 93:8382. doi:10.1063/1.1555975

Leitao DC, Gameiro L, Silva AV, Cardoso S, Freitas PP (2012) Field detection in spin valve sensors using CoFeB/Ru synthetic-antiferromagnetic multilayers as magnetic flux concentrators. IEEE Trans Mag 48:3847–3850. doi:10.1109/TMAG.2012.2195302

Marinho Z, Cardoso S, Chaves R, Ferreira R, Melo LV, Freitas PP (2011) Three dimensional magnetic flux concentrators with improved efficiency for magnetoresistive sensors. J Appl Phys 109:07E521. doi:10.1063/1.3556946

Mazumdar D, Liu X, Schrag BD, Shen W, Carter M, Xiao G (2007) Thermal stability, sensitivity, and noise characteristics of MgO-based magnetic tunnel junctions. J Appl Phys 101:09B502. doi:10.1063/1.2710953

Pannetier M, Fermon C, Le Goff G, Simola J, Kerr E (2004) Femtotesla magnetic field measurement with magnetoresistive sensors. Science 304:1648. doi:10.1126/science.1096841

Pannetier-Lecoeur M, Parkkonen L, Sergeeva-Chollet N, Polovy H, Fermon C, Fowley C (2011) Magnetocardiography with sensors based on giant magnetoresistance. Appl Phys Lett 98:153705. doi:10.1063/1.3575591

Prieto JL, Evetts JE, Blamire MG, Rouse N (2002) Development of an integrated magnetic sensor with linear output based on spin valves. J Appl Phys 91:8578. doi:10.1063/1.1447297

Stutzke NA, Russek SE, Pappas DP, Tondra M (2005) Low-frequency noise measurements on commercial magnetoresistive magnetic field sensors. J Appl Phys 97:10Q107. doi:10.1063/1.1861375

Trindade IG, Fermento R, Sousa JB, Chaves RC, Cardoso S, Freitas PP (2008) Linear field amplification for magnetoresistive sensors. J Appl Phys 103:103914. doi:10.1063/1.2936315

Trindade IG, Leitao DC, Pogorelov Y, Sousa JB, Chaves RC, Cardoso S, Freitas PP (2009) Control of hysteretic behavior in flux concentrators. Appl Phys Lett 94:073501. doi:10.1063/1.3081012

Tsang C, Krounbi M, Kasiraj P, Lee R (1992) Study of recessed MR sensors with unlaminated and multi-laminated flux-guides. IEEE Trans Magn 28:2289. doi:10.1109/20.179471

Wisniowski P, Cardoso S, Barradas N, Freitas PP (2008) Effect of free layer thickness and shape anisotropy on the transfer curves of MgO magnetic tunnel junctions. J Appl Phys 103:07A910. doi:10.1063/1.2838626

Yamada K, Maruyama T, Tatsumi T, Suzuki T, Shimabayashi K, Motomura Y, Aoyama M, Urai H (1990) Shielded magnetoresistive head for high density recording. IEEE Trans Magn 26:3010. doi:10.1109/20.102882

Yuan GL, Liu JM, Zhou L, Zhang ST, Chen XY, Liu ZG (2002) Film heterostructure with soft ferromagnetics to enhance low-field magnetoresistance. Appl Phys Lett 81:4073. doi:10.1063/1.1522130